Supporting Information

A novel magnesium metal−organic framework as a multi-responsive luminescent sensor for Fe(III) ions, pesticide and antibiotics with high selectivity and sensitivity

Ning Xu, Qinghua Zhang, Baoshan Hou, Qian Cheng, and Guoan Zhang[*]

Key Laboratory of Material Chemistry for Energy Conversion and Storage, Ministry of Education, Hubei Key Laboratory of Materials Chemistry and Service Failure, School of Chemistry and Chemical Engineering, Huazhong University of Science and Technology, Wuhan 430074, P.R. China

E-mail: zhangguoan@gmail.com (G. A. Zhang), Tel.: +86-27-87559068; Fax: +86-27-87543632

Contents

Section 1. Synthesis of H_2APDA

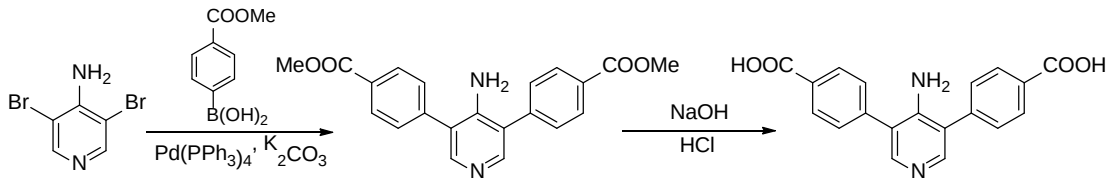

Scheme S1. The synthetic route for the H_2APDA ligand.

(a) Dimethyl 4,4'-(4-aminopyridine-3,5-diyl)dibenzoate

3,5-dibromopyridin-4-amine (1.26 g, 5.00 mmol), methyl 4-boronobenzoate (2.16 g, 12.00 mmol), $Pd(PPh_3)_4$ (0.29 g, 0.25 mmol) and K_2CO_3 (3.32 g, 24.00 mmol) were mixed in a 100 mL Schlenk flask. After vacuumized and refilled with N_2 for three times, toluene-ethanol-water (30 ml, 15 ml, 15 ml) was added. The mixture was stirred at 75 ^oC for 24 h and then cooled to room temperature. After removing the organic phase under vacuum, dichloromethane (100 mL) and H_2O (50 mL) were added. The organic phase was separated and then the aqueous phase was extracted three times with dichloromethane (60 mL). The combined organic phases were washed with saturated brine, dried over anhydrous $MgSO_4$. After removing the organic solvent by rotary evaporation, the residue was purified by column chromatography with dichloromethane /ethyl acetate (3/1, v/v) as eluent to obtain a light yellow solid product (1.45 g, 80.0% yield). ^1H NMR (400 MHz, $CDCl_3$): δ (ppm)= 3.960 (s, 6H), 4.498 (s, 2H), 7.570 (d, 4H), 8.184 (t, 6H).

(b) 4,4'-(4-aminopyridine-3,5-diyl)dibenzoic acid (H_2APDA)

1.45 g (4.00 mmol) of dimethyl 4,4'-(4-aminopyridine-3,5-diyl)dibenzoate was dissolved in THF (60 mL), and then 80 mL 2 M NaOH aqueous solution was added. The solution

was stirred at 60 ^{o}C for 6 h and the THF was removed in vacuum. Concentrated hydrochloric acid was added to the remaining aqueous solution until the solution became acidic (pH = 2~3). The solid was collected by filtration, washed several times with distilled water, and dried under vacuum to give a light yellow solid product (1.24 g, 92.7% yield). IR (KBr, cm^{-1}): 3439 (w), 3339 (w), 3073 (w), 1711 (s), 1645 (s), 1615 (s), 1481 (w), 1409 (w), 1382 (w), 1261 (m), 1228 (m), 1121 (w), 787 (w), 760 (w). ^{1}H NMR (400 MHz, DMSO-d_6): δ (ppm)= 7.125 (s, 2H), 7.652 (d, 4H), 8.094 (d, 4H), 8.213 (s, 2H), 13.320 (s, 2H).

Section 2. Crystallographic data and structural information

Table S1. The crystal data and structure refinement for Mg-APDA.

Compound	Mg-APDA
Empirical formula	$C_{38}H_{30}Mg_2N_4O_{11}$
Formula weight	767.28
Crystal system	Triclinic
Space group	*P*-1
a (Å)	13.033(6)
b (Å)	18.532(9)
c (Å)	18.881(9)
α (°)	60.752(7)
β (°)	80.205(8)
γ (°)	77.194(7)
V (Å^3)	3870(3)
Z	2
D_c/(g cm^{-3})	0.658
μ/(mm^{-1})	0.063
F(000)	796
θ range (°)	1.28-25.50
Reflections collected	14333
Parameters	496
T (K)	100(2)
GOF on F_2	0.710
R indices [$I > 2\sigma(I)$]	R_1 = 0.0876
	wR_2 = 0.1944
R indices (all data)	R_1 = 0.1688
	wR_2 = 0.2169

Table S2. Selected bond lengths (Å) and angles (deg) for Mg-APDA.

Mg-APDA			
Mg(1)-O(2)	2.016(3)	Mg(1)-O(8)#1	2.017(4)
Mg(1)-O(7)	2.053(4)	Mg(1)-O(4)#2	2.065(3)
Mg(1)-O(5)	2.133(3)	Mg(1)-N(1)#3	2.168(4)
Mg(2)-O(1)	2.016(3)	Mg(2)-O(11)#4	2.059(4)
Mg(2)-O(9)#1	2.062(3)	Mg(2)-O(6)	2.067(4)
Mg(2)-O(5)	2.121(3)	Mg(2)-N(3)	2.239(4)
O(2)-Mg(1)-O(8)#1	92.69(14)	O(2)-Mg(1)-O(7)	86.86(14)
O(8)#1-Mg(1)-O(7)	179.37(18)	O(2)-Mg(1)-O(4)#2	176.70(16)
O(8)#1-Mg(1)-O(4)#2	90.56(14)	O(7)-Mg(1)-O(4)#2	89.89(14)
O(2)-Mg(1)-O(5)	91.84(12)	O(8)#1-Mg(1)-O(5)	86.27(13)
O(7)-Mg(1)-O(5)	94.20(15)	O(4)#2-Mg(1)-O(5)	87.83(12)
O(2)-Mg(1)-N(1)#3	91.48(14)	O(8)#1-Mg(1)-N(1)#3	85.18(15)
O(7)-Mg(1)-N(1)#3	94.37(17)	O(4)#2-Mg(1)-N(1)#3	89.34(14)
O(5)-Mg(1)-N(1)#3	170.96(15)	O(1)-Mg(2)-O(11)#4	90.08(13)
O(1)-Mg(2)-O(9)#1	98.17(13)	O(11)#4-Mg(2)-O(9)#1	171.32(14)
O(1)-Mg(2)-O(6)	88.85(15)	O(11)#4-Mg(2)-O(6)	88.72(15)
O(9)#1-Mg(2)-O(6)	94.09(14)	O(1)-Mg(2)-O(5)	93.86(14)
O(11)#4-Mg(2)-O(5)	87.36(14)	O(9)#1-Mg(2)-O(5)	89.40(12)
O(6)-Mg(2)-O(5)	175.24(14)	O(1)-Mg(2)-N(3)	172.98(14)
O(11)#4-Mg(2)-N(3)	85.71(13)	O(9)#1-Mg(2)-N(3)	86.33(13)
O(6)-Mg(2)-N(3)	85.45(15)	O(5)-Mg(2)-N(3)	91.56(14)

Symmetry transformations used to generate equivalent atoms:

#1 -*x*+1,-*y*+2,-z+1 #2 *x*,*y*,*z*+1 #3 -*x*+2,-*y*+2,-*z* #4 -*x*+1,-*y*+1,-*z*+1

Section 3. General characterizations

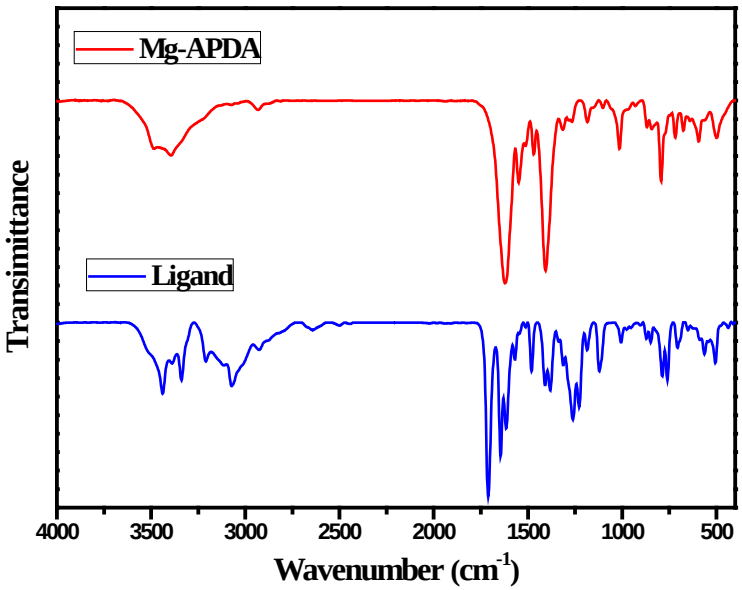

Figure S1. IR spectra of the free ligand and Mg-APDA.

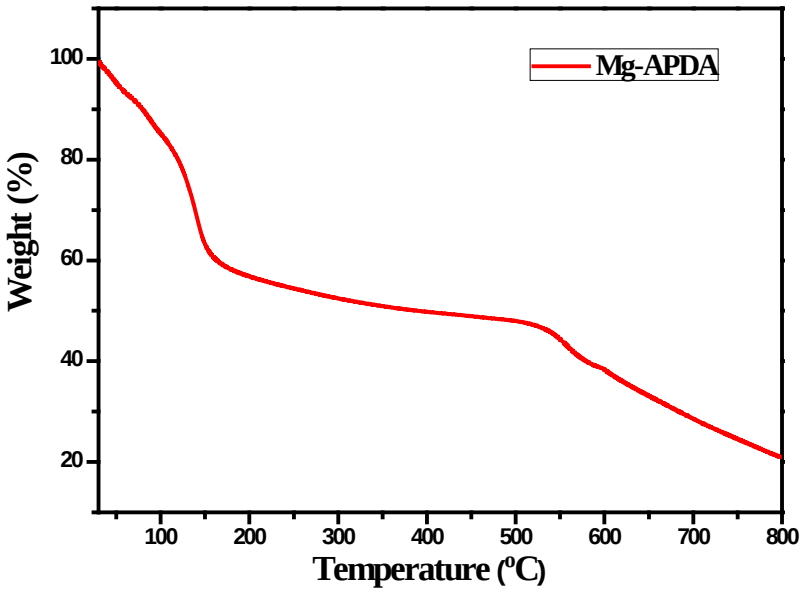

Figure S2. TGA curve of Mg-APDA.

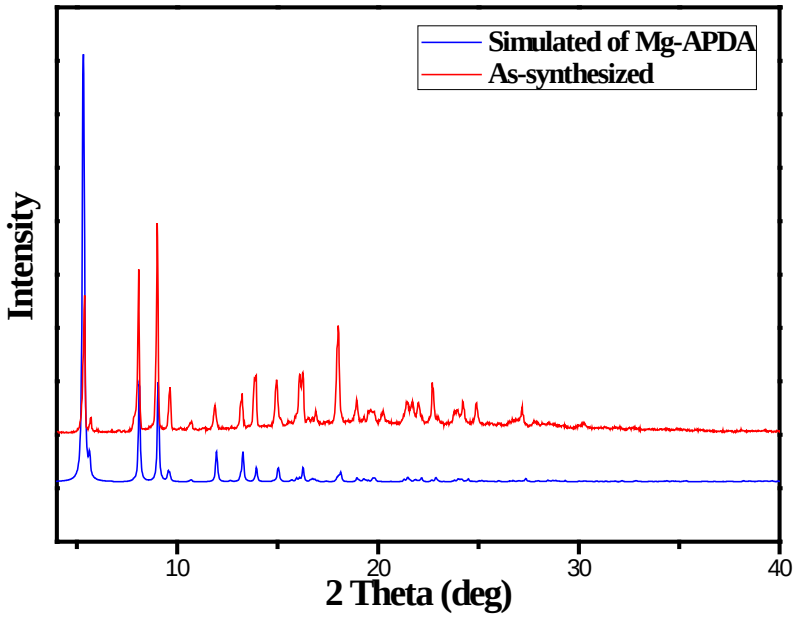

Figure S3. XRD patterns of Mg-APDA.

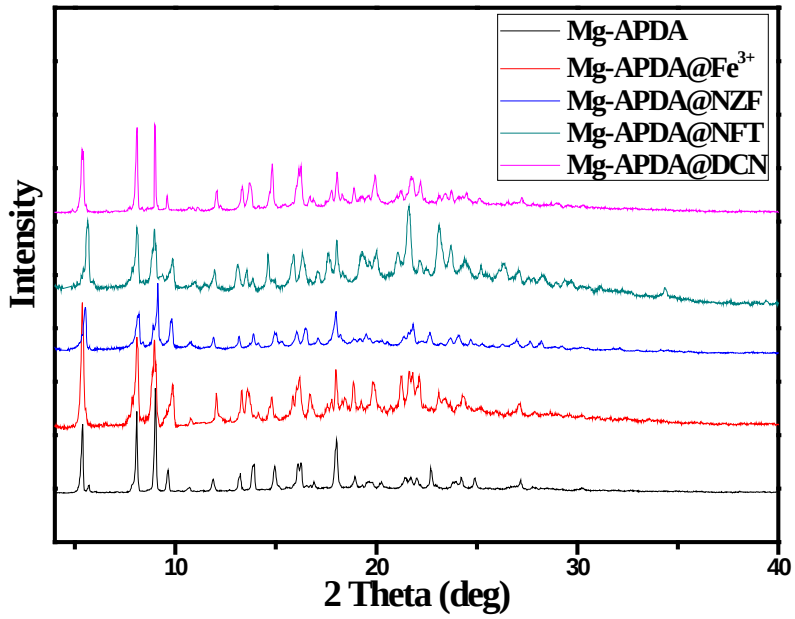

Figure S4. PXRD patterns of Mg-APDA after immersed in the DMF solution (1.0 mM) with different analytes (Fe(III), nitrofurazone (NZF), nitrofurantoin (NFT) and 2,6-dichloro-4-nitroaniline (DCN)) for 6 hours.

Section 4. Detection of metal ions

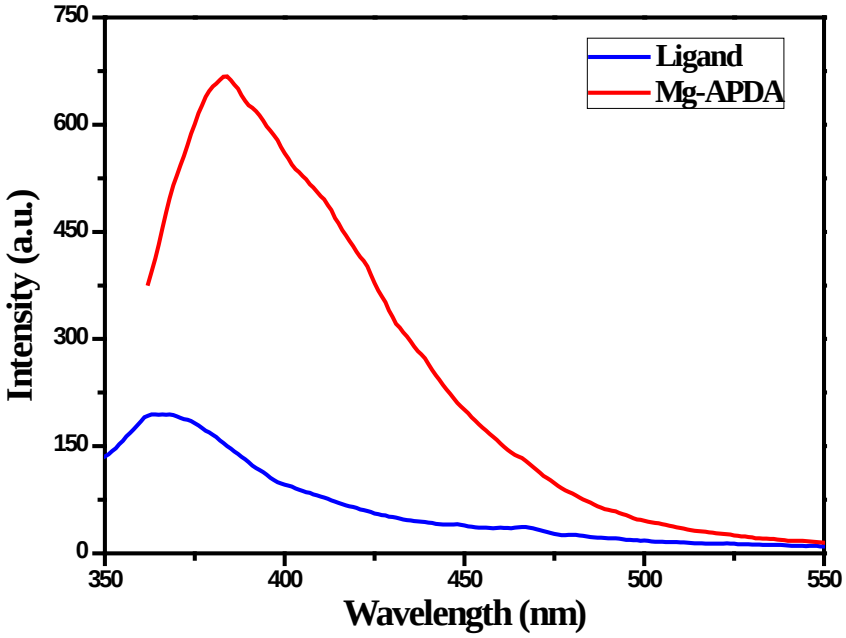

Figure S5. Solid-state luminescence spectra of the free ligand and Mg-APDA.

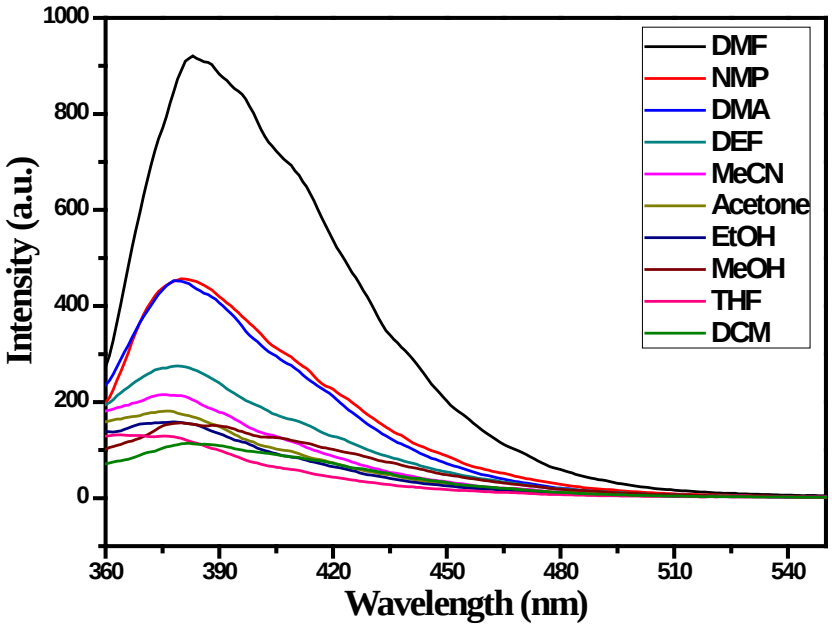

Figure S6. Fluorescence spectra of Mg-APDA dispersed in different solvents.

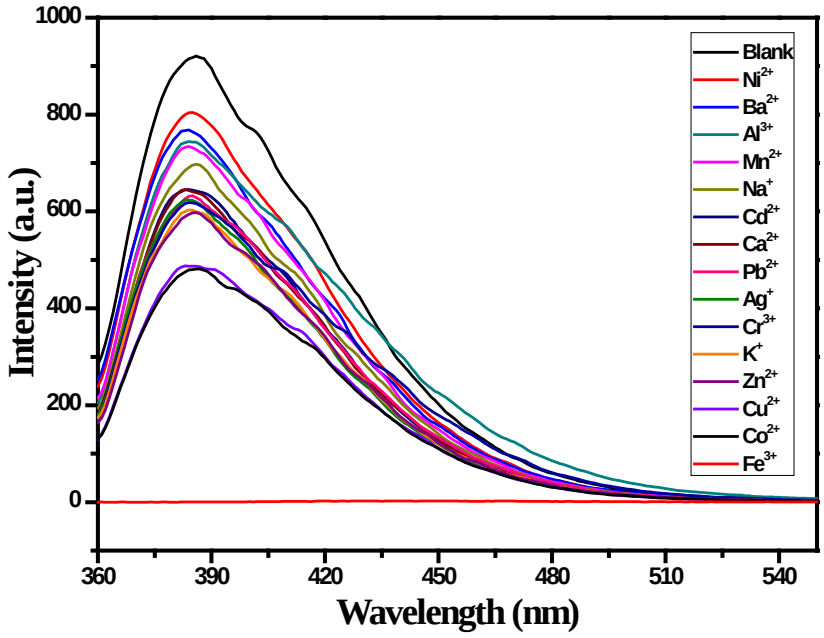

Figure S7. Fluorescence spectra of Mg-APDA dispersed in various 1 mM metal ions.

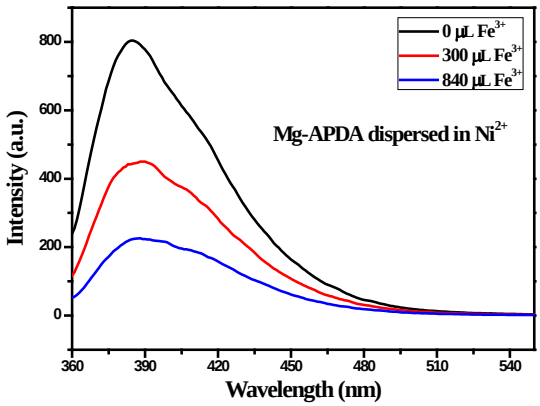
0 μL Fe3+
300 μL Fe3+
840 μL Fe3+
Mg-APDA dispersed in Ni2+
Intensity (a.u.)
Wavelength (nm)

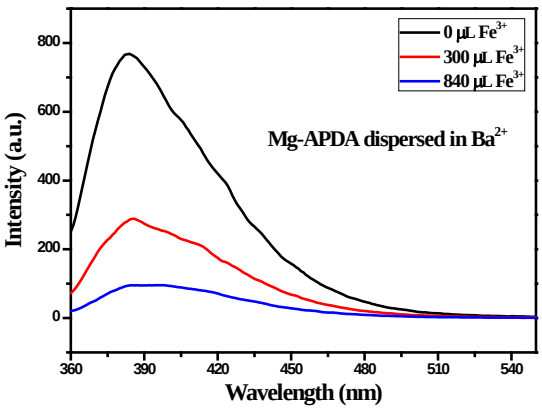
0 μL Fe3+
300 μL Fe3+
840 μL Fe3+
Mg-APDA dispersed in Ba2+
Intensity (a.u.)
Wavelength (nm)

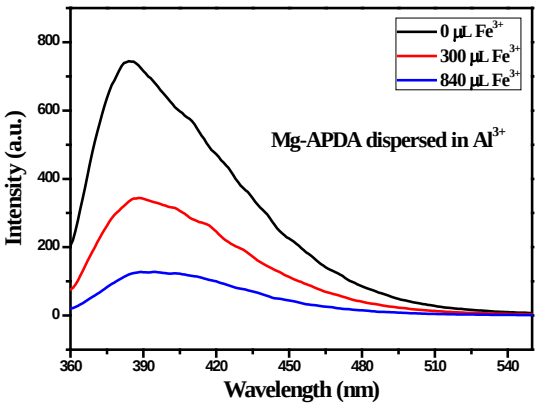
0 μL Fe3+
300 μL Fe3+
840 μL Fe3+
Mg-APDA dispersed in Al3+
Intensity (a.u.)
Wavelength (nm)

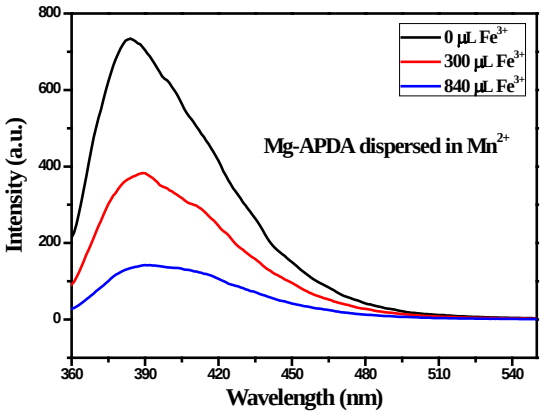
0 μL Fe3+
300 μL Fe3+
840 μL Fe3+
Mg-APDA dispersed in Mn2+
Intensity (a.u.)
Wavelength (nm)

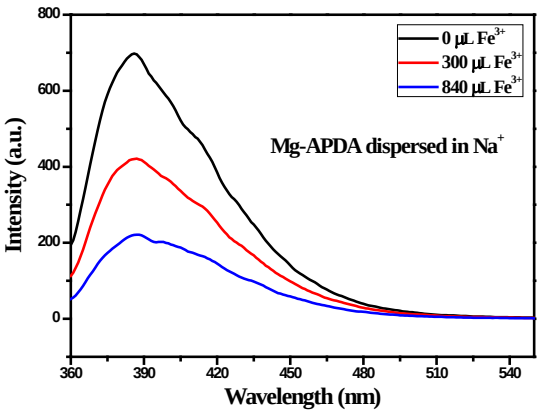
0 μL Fe3+
300 μL Fe3+
840 μL Fe3+
Mg-APDA dispersed in Na+
Intensity (a.u.)
Wavelength (nm)

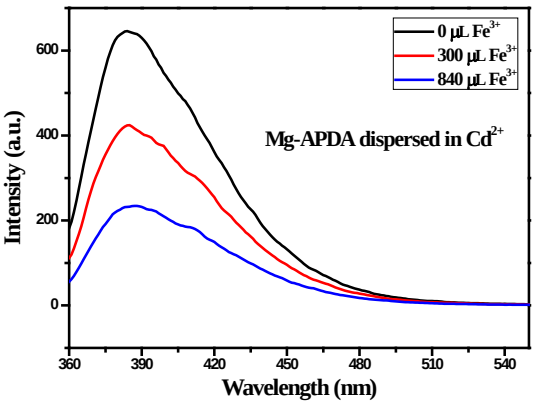
0 μL Fe3+
300 μL Fe3+
840 μL Fe3+
Mg-APDA dispersed in Cd2+
Intensity (a.u.)
Wavelength (nm)

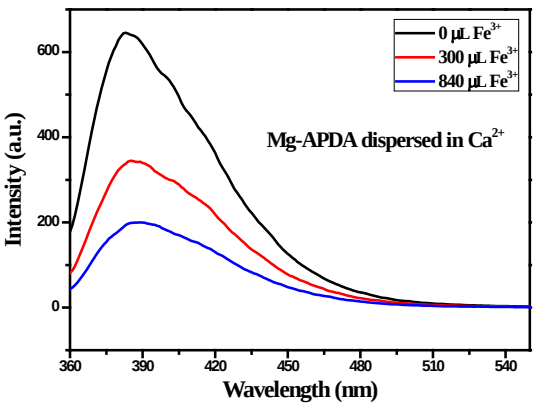
0 μL Fe3+
300 μL Fe3+
840 μL Fe3+
Mg-APDA dispersed in Ca2+
Intensity (a.u.)
Wavelength (nm)

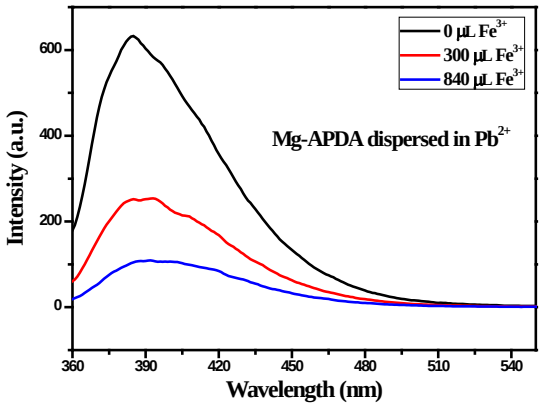
0 μL Fe3+
300 μL Fe3+
840 μL Fe3+
Mg-APDA dispersed in Pb2+
Intensity (a.u.)
Wavelength (nm)

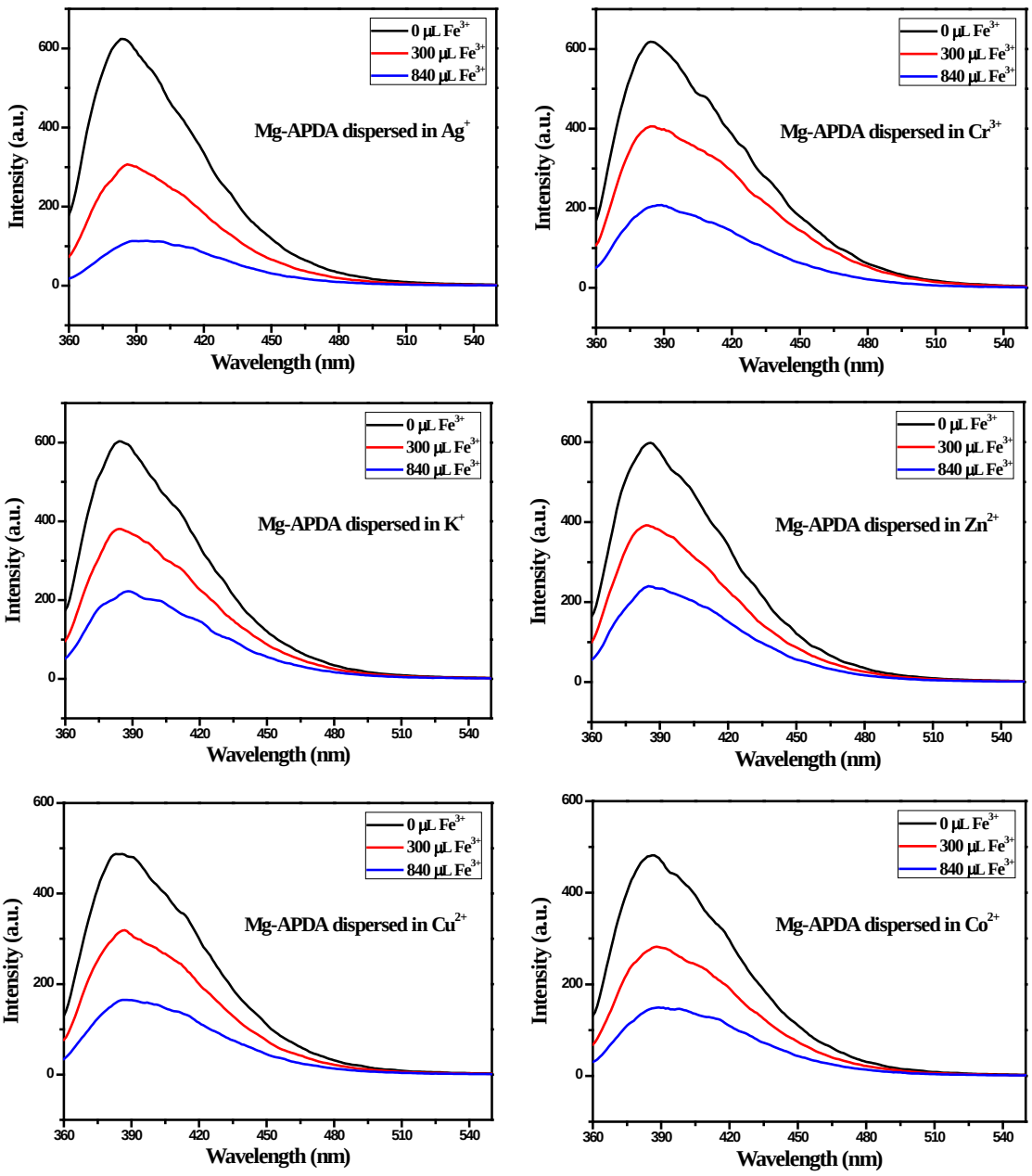

Figure S8. Fluorescence spectra of Mg-APDA dispersed in different interfering metal ions with adding various amount of 1 mM Fe^{3+}.

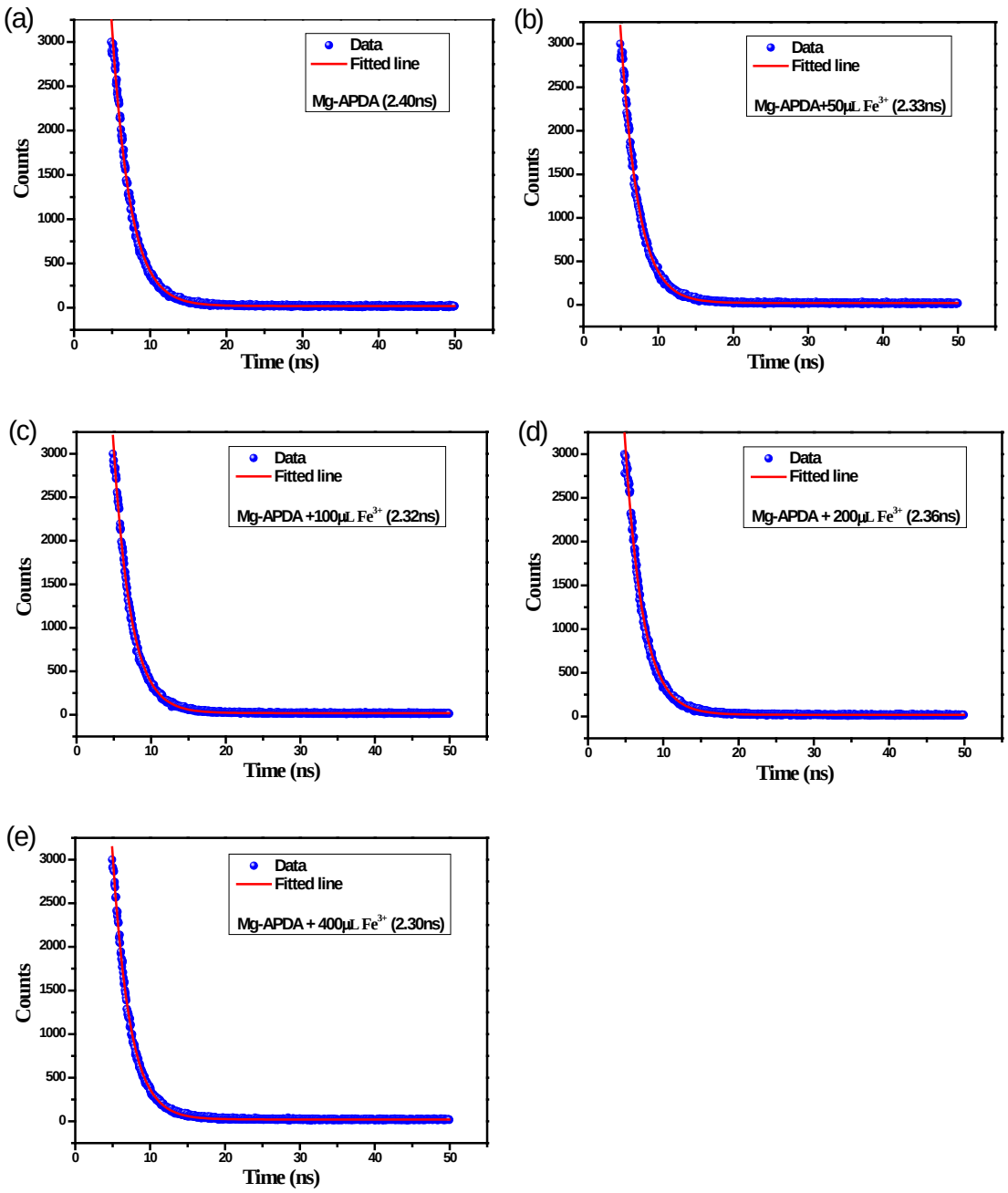

Figure S9. (a) Luminescence decay curve of Mg-APDA in DMF. (b-e) Luminescence decay curve of Mg-APDA in DMF with different amount of 1 mM Fe^{3+}.

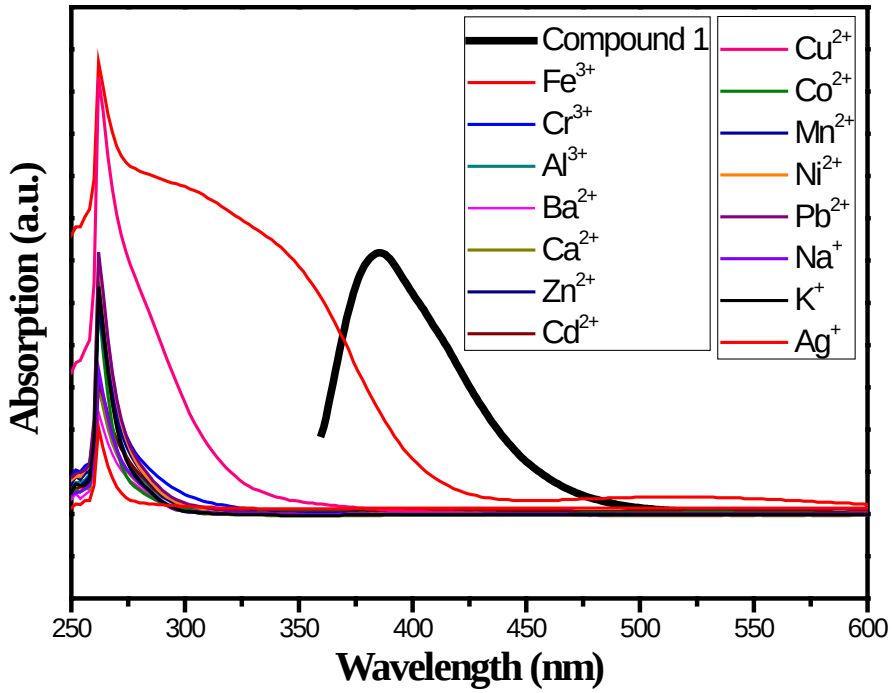

Figure S10. UV-vis absorption spectra of varied metal ions (0.1 mM) and the normalized emission spectra of Mg-APDA in DMF.

Table S3. Performance comparison between various MOF fluorescent sensors for the detection of Fe^{3+} ions.

LMOFs	K_{sv} (M^{-1})	Detection limits (μM)	Ref.
$\{[Zn(\mu\text{-HCIP})(\mu\text{-pbix})]\cdot 2H_2O\}_n$	6.87×10^3	3.72	1
$[Zn_2(TPOM)(NDC)_2]\cdot 3.5H_2O$	1.9×10^4	2	2
$\{(NH_4)_2\cdot Q[6]\cdot(HDTNB)_2\cdot 2H_2O\}$	1.745×10^3	---	3
$[Cd_2(L)(Hbptc)_2]$	1.94×10^4	2.38	4
$\{[Tb_4(OH)_4(DSOA)_2(H_2O)_8]\cdot(H_2O)_8\}_n$	3.54×10^3	---	5
$[Cd(L^1)(oba)]\cdot DMF$	2.69×10^4	1.95	6
$[Eu(Hpzbc)_2(NO_3)]\cdot H_2O$	---	26	7
$\{[Eu_2L_{1.5}(H_2O)_2EtOH]\cdot DMF\}_n$	2.942×10^3	10	8
$\{[Cd_2(bptc)(2,2'\text{-bipy})_2(H_2O)_2]\}_n$	8.61×10^3	10.2	9
$\{[Tb(L)_{1.5}(H_2O)]\cdot 4H_2O\}_n$	---	4.1	10
Mg-APDA	2.06×10^4	2.58	This work

Section 5. Detection of antibiotics

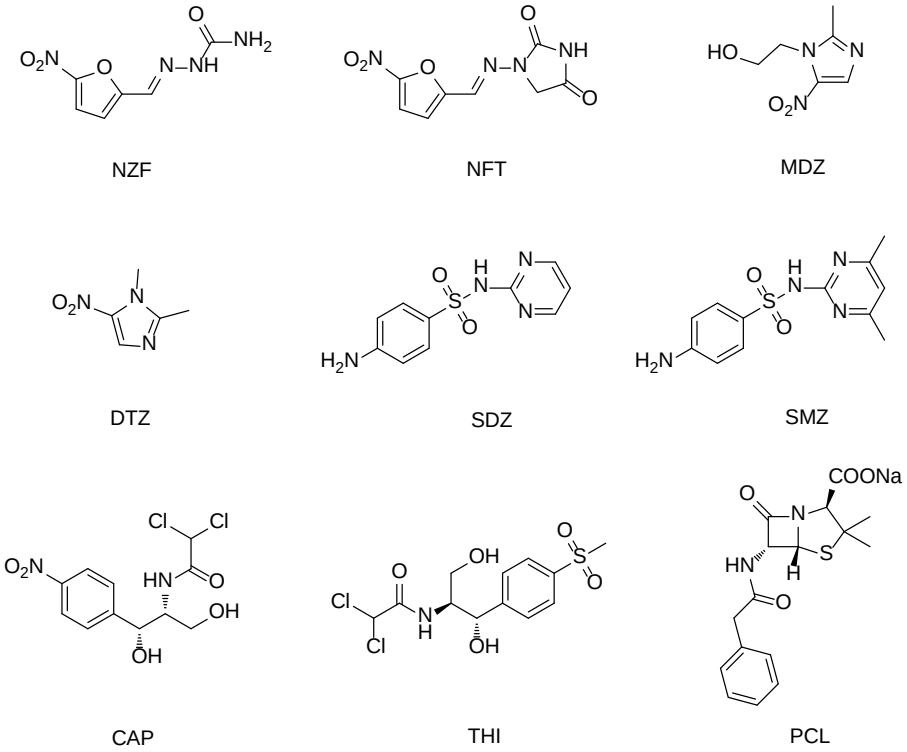

Scheme S2. Chemical structures of the antibiotics investigated.

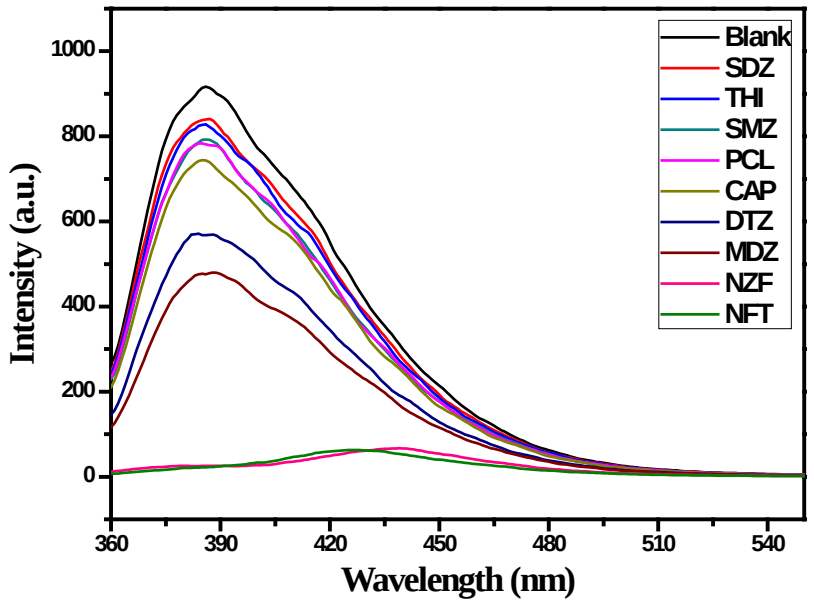

Figure S11. Fluorescence spectra of Mg-APDA dispersed in various 0.1 mM antibiotics.

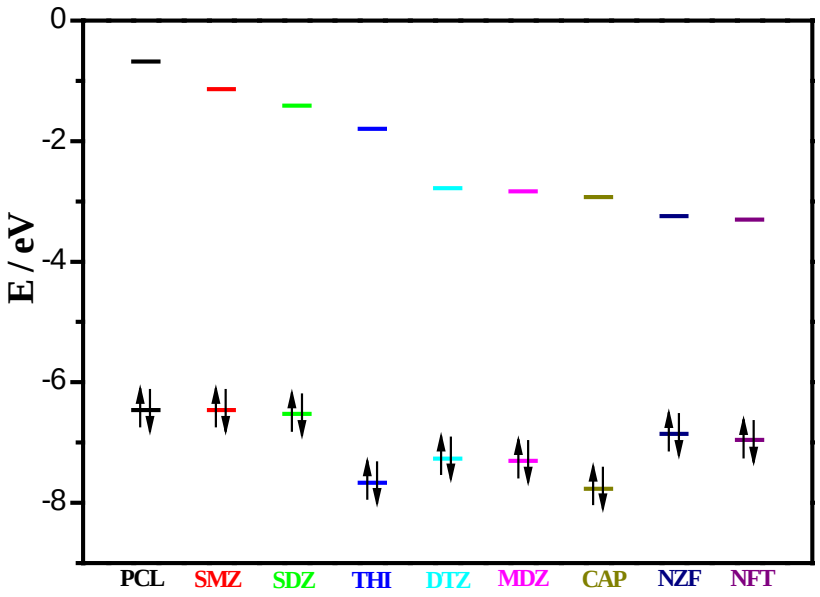

Figure S12. HOMO and LUMO energies of the selected antibiotics calculated by density functional theory (DFT) with B3LYP/6-31+G* basis set.

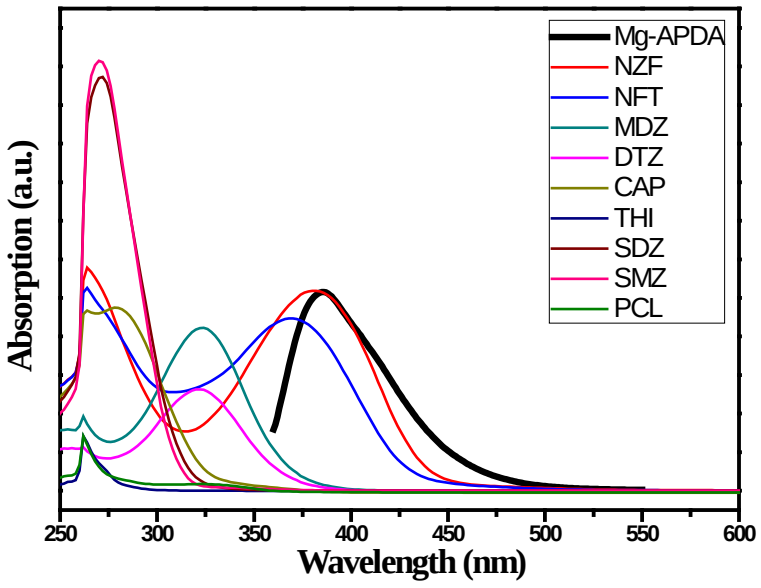

Figure S13. UV-vis absorption spectra of selected antibiotics (0.1 mM) and the normalized emission spectra of Mg-APDA in DMF.

Table S4. Comparison of detection limits among other reported MOF materials and Mg-APDA as the NZF/NFT sensor.

MOFs	Name	Analyte	K_{sv} (M^{-1})	Detection limits (ppb)	Ref.
Zr(IV)-Based MOFs	BUT-12	NZF	1.1×10^5	58	11
	BUT-13	NZF	7.5×10^4	90	
Cd(II)-Based MOFs	Sample 3	NZF	5.06×10^4	162	12
		NFT	3.57×10^4	274	
	Sample 4	NZF	1.04×10^5	75	
		NFT	7.19×10^4	131	
	Sample 5	NZF	1.33×10^5	60	
		NFT	6.93×10^4	142	
In(III)-Based MOF	V102	NZF	6.38×10^4	200	13
Zn(II)-Based MOF	Sample 1	NZF	---	100	14
Mg(II)-Based MOF	Mg-APDA	NZF	9.00×10^4	108	This work
		NFT	8.82×10^4	126	

Table S5. HOMO and LUMO energies for the selected antibiotics calculated by density functional theory (DFT) with B3LYP/6-31+G* basis set.

Analytes	HUMO (eV)	LUMO (eV)	Band Gap (eV)
PCL	-6.46285	-0.67812	5.78473
SMZ	-6.46258	-1.13773	5.32485
SDZ	-6.52544	-1.40958	5.11586
THI	-7.66671	-1.79735	5.86936
DTZ	-7.26914	-2.78052	4.48862
MDZ	-7.30669	-2. 83495	4.47174
CAP	-7.76821	-2. 92992	4.83829
NZF	-6.85634	-3.24612	3.61022
NFT	-6.95838	-3.30218	3.6562

Section 6. Detection of pesticide

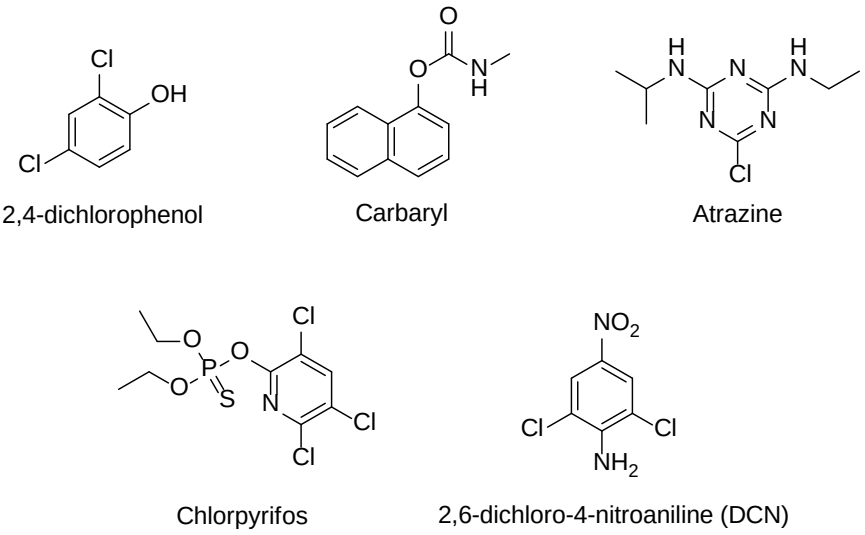

Scheme S3. The chemical structures of pesticides investigated.

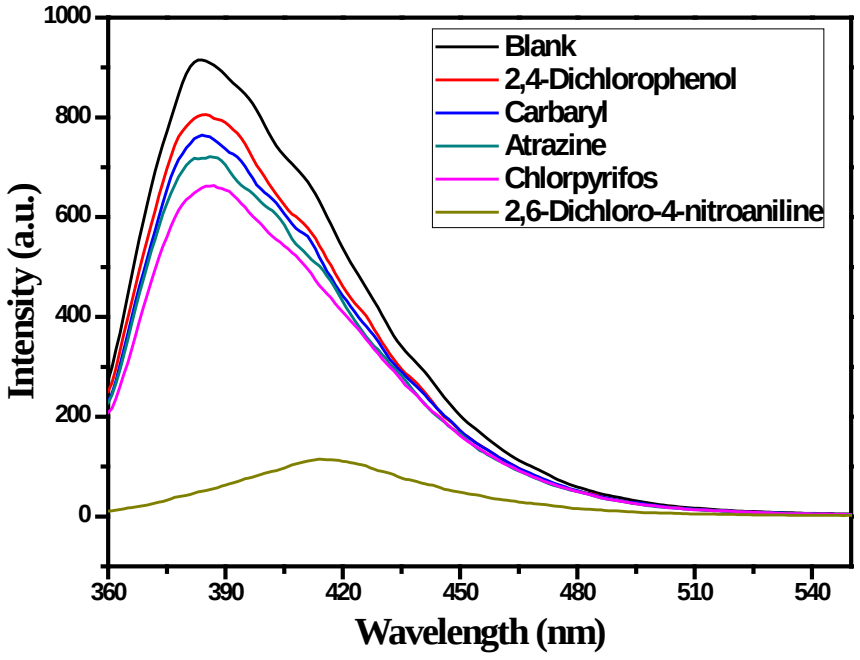

Figure S14. Fluorescence spectra of Mg-APDA dispersed in various 0.1 mM pesticides.

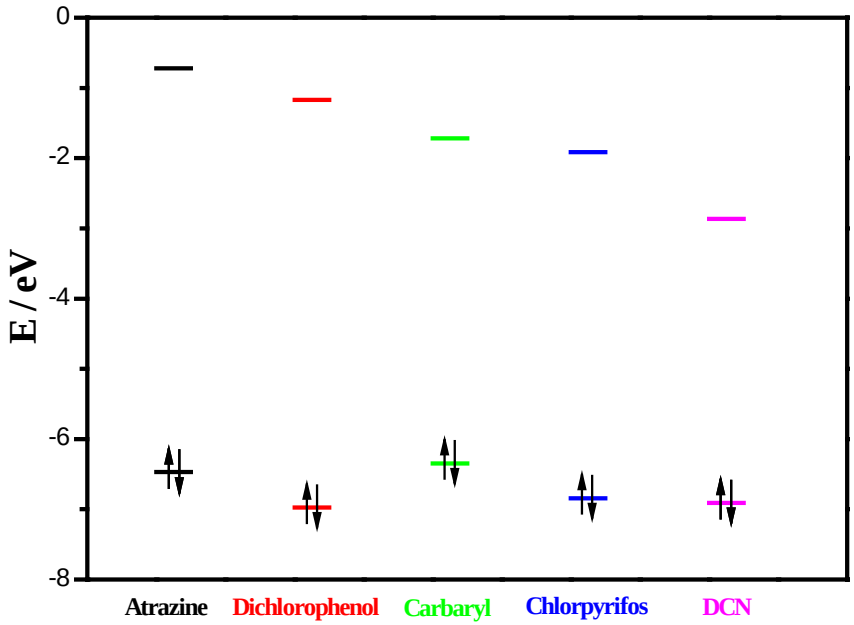

Figure S15. HOMO and LUMO energies of the selected pesticides calculated by density functional theory (DFT) with B3LYP/6-31+G* basis set.

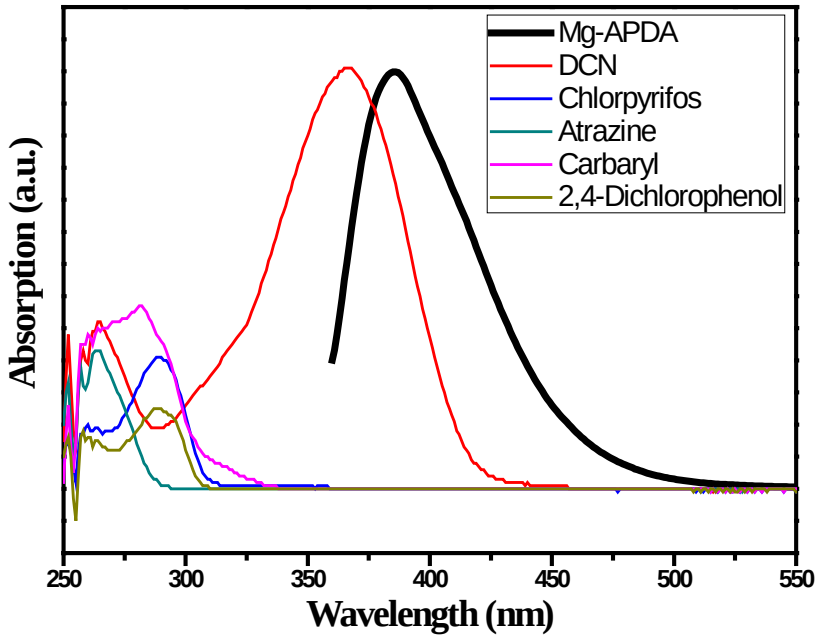

Figure S16. UV-vis absorption spectra of selected pesticides (0.1 mM) and the normalized emission spectra of Mg-APDA in DMF.

Table S6. HOMO and LUMO energies for the selected pesticides calculated by density functional theory (DFT) with B3LYP/6-31+G* basis set.

Analytes	HUMO (eV)	LUMO (eV)	Band Gap (eV)
Atrazine	-6.46802	-0.7203	5.74772
2,4-Dichlorophenol	-6.97525	-1.16821	5.80704
Carbaryl	-6.34747	-1.72007	4.6274
Chlorpyrifos	-6.84436	-1.91681	4.92755
DCN	-6.90994	-2.8657	4.04424

References

(1) Arici, M. r. Luminescent 2D + 2D → 2D interpenetrated Zn(II)-coordination polymer based on reduced schiff base tricarboxylic acid and bis(imidazole) ligand for detection of picric acid and Fe^{3+} ions. *Cryst. Growth Des.* **2017,** *17*, 5499-5505.

(2) Lv, R.; Li, H.; Su, J.; Fu, X.; Yang, B.; Gu, W.; Liu, X. Zinc metal-organic framework for selective detection and differentiation of Fe(III) and Cr(VI) ions in aqueous solution. *Inorg. Chem.* **2017,** *56*, 12348-12356.

(3) Zhang, X.-D.; Zhao, Y.; Chen, K.; Wang, P.; Kang, Y.-S.; Wu, H.; Sun, W.-Y. Cucurbit[6]uril-based multifunctional supramolecular assemblies: synthesis, removal of Ba(II) and fluorescence sensing of Fe(III). *Dalton Trans.* **2018,** 47, 3958-3964.

(4) Liu, Z. Q.; Zhao, Y.; Zhang, X. D.; Kang, Y. S.; Lu, Q. Y.; Azam, M.; Alresayes, S. I.; Sun, W. Y. Metal-organic frameworks with 1,4-di(1H-imidazol-4-yl)benzene and varied carboxylate ligands for selectively sensing Fe(III) ions and ketone molecules. *Dalton Trans.* **2017,** *46*, 13943-13951.

(5) Dong, X.-Y.; Wang, R.; Wang, J.-Z.; Zang, S.-Q.; Mak, T. C. Highly selective Fe^{3+} sensing and proton conduction in a water-stable sulfonate-carboxylate Tb-organic-framework. *J. Mater. Chem. A* **2015,** *3*, 641-647.

(6) Liu, Z. Q.; Chen, K.; Zhao, Y.; Kang, Y. S.; Liu, X. H.; Lu, Q. Y.; Azam, M.; Alresayes, S. I.; Sun, W. Y. Structural diversity and sensing properties of metal-organic frameworks with multicarboxylate and 1H-imidazol-4-yl-containing ligands. *Cryst. Growth Des.* **2018,** *18*, 1136-1146.

(7) Li, G.-P.; Liu, G.; Li, Y.-Z.; Hou, L.; Wang, Y.-Y.; Zhu, Z. Uncommon pyrazoyl-carboxyl bifunctional ligand-based microporous lanthanide systems: sorption and luminescent sensing properties. *Inorg. Chem.* **2016,** *55*, 3952-3959.

(8) Liu, W.; Huang, X.; Xu, C.; Chen, C.; Yang, L.; Dou, W.; Chen, W.; Yang, H.; Liu, W. A multi-responsive regenerable europium-organic framework luminescent sensor for Fe^{3+}, Cr^{VI} anions, and picric acid. *Chem. – Eur. J.* **2016,** *22*, 18769-18776.

(9) Lin, Y.; Zhang, X.; Chen, W.; Shi, W.; Cheng, P. Three cadmium coordination polymers with carboxylate and pyridine mixed ligands: luminescent sensors for Fe^{III} and Cr^{VI} Ions in an aqueous

medium. *Inorg. Chem.* **2017,** *56*, 11768-11778.

(10) Li, Z.-J.; Li, X.-Y.; Yan, Y.-T.; Hou, L.; Zhang, W.-Y.; Wang, Y.-Y. Tunable emission and selective luminescence sensing in a series of lanthanide metal-organic frameworks with uncoordinated lewis basic triazolyl sites. *Cryst. Growth Des.* **2018,** *18*, 2031-2039.

(11) Wang, B.; Lv, X.-L.; Feng, D.; Xie, L.-H.; Zhang, J.; Li, M.; Xie, Y.; Li, J.-R.; Zhou, H.-C. Highly stable Zr(IV)-based metal-organic frameworks for the detection and removal of antibiotics and organic explosives in water. *J. Am. Chem. Soc.* **2016,** *138*, 6204-6216.

(12) Zhao, D.; Liu, X.-H.; Zhao, Y.; Wang, P.; Liu, Y.; Azam, M.; Al-Resayes, S. I.; Lu, Y.; Sun, W.-Y. Luminescent Cd(II)-organic frameworks with chelating NH_2 sites for selective detection of Fe(III) and antibiotics. *J. Mater. Chem. A* **2017,** *5*, 15797-15807.

(13) Hou, S.-L.; Dong, J.; Jiang, X.-L.; Jiao, Z.-H.; Wang, C.-M.; Zhao, B. Interpenetration-depended luminescent probe in indium-organic frameworks for selectively detecting nitrofurazone in water. *Anal. Chem.* **2018,** *90*, 1516-1519.

(14) Liu, X.-G.; Tao, C.-L.; Yu, H.-Q.; Chen, B.; Liu, Z.; Zhu, G.-P.; Zhao, Z.; Shen, L.; Tang, B. Z. A new luminescent metal-organic framework based on dicarboxyl-substituted tetraphenylethene for efficient detection of nitro-containing explosives and antibiotics in aqueous media. *J. Mater. Chem. C* **2018,** *6*, 2983-2988.